Bond Behaviour of Multi-Ply Steel Reinforced Grout Composites

G.E. Thermou[1*], S. De Santis[2], G. de Felice[3], S. Alotaibi[4,5],
F. Roscini[6], I. Hajirasouliha[7], M. Guadagnini[7]

Abstract

This paper presents an experimental investigation on Steel Reinforced Grout (SRG) systems comprising multiple layers of galvanized UHTSS textiles, with either 4 or 8 cords/in density, embedded within a geopolymer mortar. Lap-splice tests and single-lap bond tests were performed to develop an improved understanding of the textile-to-textile load transfer capacity and of the SRG-to-concrete substrate bond behaviour. The effects of number of textile plies, cord density and compressive strength of concrete on the bond behaviour are analysed.

Keywords: bond and interfacial stresses; digital image correlation (DIC); fabric reinforced cementitious matrix (FRCM); textile reinforced mortar (TRM); lap-splice test; shear bond test; strengthening.

1 Introduction

Aging of the structures due to the continuous deterioration caused by environmental conditions and extreme events (e.g., earthquakes) can significantly affect their structural performance and resilience over time [1]. Changes in use or, as for infrastructures, increasing traffic volumes, may also result in increasing load demands. Additionally, updating building codes generally corresponds to rising required safety, such that existing structures may become

[1]Assistant Professor, University of Nottingham, Nottingham, UK
[2] Assistant Professor, Roma Tre University, Rome, Italy
[3] Professor, Roma Tre University, Rome, Italy
[4] Lecturer, Shaqra University, Dawadmi, Saudi Arabia
[5] PhD student, The University of Sheffield, Sheffield, UK
[6] Marie Curie IF, The University of Sheffield, Sheffield, UK
[7] Senior Lecturer, The University of Sheffield, Sheffield, UK
[*] Corresponding author; georgia.thermou@nottingham.ac.uk

noncompliant with the most recent standards. When demolition is not an option due to either the prohibitive cost or the cultural and historical significance of the structure, retrofitting is the only solution. Depending on the performance targets and level of retrofitting, global or local intervention methods could be selected [2]. In the past three decades, the use of Fibre Reinforced Polymers (FRPs) has emerged as one of the most effective local strengthening methods. Nevertheless, FRPs have shown some drawbacks, such as high cost, poor fire resistance, lack of vapour permeability, toxic nature of epoxy, and lack of reversibility [3-4]. In order to overcome many of these drawbacks, closely related to the use of an organic matrix as the bonding material, a new generation of composites, named as Fabric Reinforced Cementitious Matrix (FRCM), has been developed, in which inorganic matrices are used instead of resins [4-5].

The experimental studies performed in the last 15 years on the bond behaviour of FRCM systems have identified the complexity of the FRCM-to-substrate shear transfer mechanisms and the occurrence of multiple failure modes [5-7]. In the case of Steel Reinforced Grout (SRG) systems, which comprise unidirectional textiles of ultra-high tensile strength steel (UHTSS) cords, studies on bond behaviour have been conducted on both concrete [3, 8-10] and masonry [1, 5-6, 11-14] substrates. Different parameters have been investigated, such as the bond length [3, 13], the fabric density [1, 14], the surface preparation [3, 5], the matrix strength [6], the substrate strength [12] and the substrate curvature [13]. In general, in the previous studies the failure of FRCM systems can occur due to: (i) debonding either at the fabric-to-matrix interface [3] or at the substrate-to-matrix interface, sometimes involving a thin layer of substrate (cohesive failure in substrate) [12], (ii) slippage of the fabric [15] or (iii) fabric tensile rupture [14]. De Santis and de Felice [12] attributed the debonding at the substrate-to-matrix interface to the high strength of the matrix applied to a relatively weak substrate. They observed that the substrate to matrix detachment was mainly associated with short bonded lengths. They also concluded that slippage of the fabric was attributed to its poor interlocking with the grout, as was also observed in textiles comprising stainless steel ropes, whose surface is smoother than

that of cords [1]. Some of the above-mentioned studies suggested an effective transfer length for SRG systems ranging from 150 mm to 300 mm [1, 3, 9]. Accordingly, and based also on the results of tests not only on SRG but also on other FRCM systems [16], a bond length of 300 mm is recommended by most testing guidelines [1, 17].

Despite the knowledge developed in the field of FRCM so far, all the previous studies have considered SRG systems comprising only one layer of steel textile. Nevertheless, multiple textile layers may be required in some applications, such as the flexural strengthening of large span reinforced concrete beams [18]. To date, existing knowledge on the shear transfer mechanism developed along the multiple layers of the steel fabric and on the overall behaviour of multi-ply SRG composites is still very limited, despite the crucial role it plays on the effectiveness of externally bonded reinforcements. This study aims to bridge this knowledge gap and to gain an improved understanding of the bond behaviour of multi-ply SRG reinforcements applied to concrete substrates. An experimental investigation was performed on SRG composites comprising unidirectional textiles made of galvanized UHTSS cords, with either 4 or 8 cords/in density, embedded in a geopolymer mortar, particularly suitable for strengthening of concrete elements. The effect of number of textile layers, steel cords density and compressive strength of the substrate was analysed through a series of complementary tests. Lap-splice tests were carried out to study the textile-to-textile load transfer capacity for different overlap lengths (from 100 mm to 300 mm). Additionally, single-lap shear bond tests were performed on multi-ply SRG composites (comprising 1, 2 or 3 plies) bonded to two types of concrete substrates (with a compressive strength of 14 N/mm^2 or 28 N/mm^2).

2 Materials and experimental setups

2.1 Materials

The textiles investigated in this work comprise unidirectional ultra-high tensile strength steel (UHTSS) micro-cords, thermo-welded to a fibreglass micromesh. Each cord has a cross sectional area of 0.538 mm^2 and is obtained by joining 5 wires, 3 straight and 2 wrapped with a

high torque angle to enhance the interlocking with the mortar. Wires have a cross sectional area of 0.11 mm^2 and are galvanized (coated with zinc) to improve their durability. Two different fabrics were tested, which differ only in cord density, using 4 cords/in (corresponding to 1.57 cords/cm, labelled as S4) and 8 cords/in (3.15 cords/cm; S8). In the former (S4), cords are evenly arranged such that the clear spacing between two cords is 5.45 mm, whereas, in the latter (S8), cords are paired such that the clear spacing between two pairs is 2.28 mm. S4 has a surface mass density of γ=670 g/m^2 and a design thickness of t_f=0.084 mm, whereas S8 has γ=1300 g/m^2 and t_f=0.169 mm. The textiles have an average tensile strength of about 3200N/mm^2, an ultimate strain of 2.2% and tensile modulus of elasticity of 186kN/mm^2 [1]. The matrix used to manufacture SRG composites is a pre-mixed geopolymer mortar with a crystalline reaction geo-binder base. According to manufacturer's datasheet [19], it has a compressive strength of 55 N/mm^2, tensile strength of 10 N/mm^2 and Young's modulus of 22 kN/mm^2. For manufacturing the composites, a water-to-mortar powder mix ratio of 1:5 was used.

2.2 Direct tensile tests

Direct tensile tests were carried out on prismatic specimens (coupons) with a total length of 600 mm, width of 50 mm and thickness of 10 mm. In the case of S4, the strip embedded in the coupon comprised 8 cords, whereas, in the case of S8, the strip had 16 cords. In total, 16 specimens were tested, 8 with S4 and 8 with S8. Coupons were manufactured in Perspex moulds, demoulded after 2 days, cured for 28 days in water and, finally, stored for 7 days under standard laboratory conditions before testing. Displacement controlled tests were carried out at a machine stroke displacement rate of 0.01 mm/s, using a hydraulic universal testing machine with 500 kN capacity. The specimens were gripped by the wedges of the machine, which applied a lateral pressure to avoid slippage [20]. The ends of the coupons were wrapped with glass fibre reinforced polymer (GFRP) [15] to ensure a uniform stress distribution within the loading areas and prevent mortar crushing.

The load was recorded by an integrated load cell and divided by the cross sectional area of the steel textile (4.30 mm^2 for S4 and 8.61 mm^2 for S8) to calculate the stress (f). The strain (ε_t) was derived as the mean of the displacements recorded by two transducers divided by their gauge length (200 mm). Digital image correlation (DIC) was also applied. A digital camera was placed on a stiff frame at 1.1 m distance from the specimen, to check that the sensor and the surface of the coupon were parallel. Pictures were taken every 5 seconds during test execution and post-processed to derive the displacement field. Subsequently, two points were selected on the surface of the coupon, one in the upper portion and one in the lower one, based on the crack pattern (each point was taken in the middle between two cracks). The strain was then calculated as the relative displacement between these two points divided by their initial distance and used to validate the strain obtained from the transducers [21].

Specimens were labelled using the notation "DT-X-N", in which "DT" denotes direct tensile test, "X" denotes the density of steel fabric ("4" for S4 and "8" for S8), and "N" identifies the specimen number (from 1 to 8) within a set of nominally identical specimens.

2.3 Lap-splice tests

Lap-splice tests were carried out to investigate the textile-to-textile load transfer capacity and were performed on prismatic specimens similar to those subjected to direct tensile tests. They had 600 mm total length, 50 mm width and 12 mm thickness, were cast in the same moulds and underwent the same curing process. The overlap length in the central portion of the coupon, (L') was 100 mm, 200 mm or 300 mm for different specimens (see Figure 1). The thickness of the mortar matrix between the plies along the overlap was 3 mm [9]. The symmetry along the thickness direction prevented the occurrence of parasitic bending moments caused by eccentricities. During manufacturing of the specimens, particular care was paid to align the textile strips, to keep a constant spacing between them, and to let an adequate amount of mortar pass through the voids between the cords. The ends of the specimens were wrapped with GFRP and

the tests were performed following the same protocol as for the as was used for the direct tensile tests. Five nominally identical specimens were manufactured and tested for each value of L' (15 specimens for S4 and 15 specimens for S8).

Specimens were labelled using the notation "LS-X-Y-N", in which "LS" denotes lap-splice test, "X" denotes the density of steel fabric ("4" for S4 and "8" for S8), "Y" is the overlap length in mm (100, 200 and 300), and, finally, "N" identifies the specimen number (from 1 to 5) within a set of nominally identical specimens.

2.4 Shear bond tests

Single-lap shear bond tests were performed on concrete substrates. A total of 42 plain concrete prisms with a length of 500 mm and a cross section of 150 mm × 150 mm (Figure 2(a)) were cast in two different batches. Half of the concrete prisms were characterised by low compressive strength (L - 14 N/mm^2) and the remaining half by a medium compressive strength (M - 28 N/mm^2). The 14 N/mm^2 concrete compressive strength is representative of structures built in the first half of the 20th century where concrete quality of construction materials was rather low [22].

SRG strips were bonded over a 300 mm long and 100 mm wide area. As shown in Figure 3(a), the bonded area was on the vertical face to one of the sides of the prism (perpendicular to the casting face) and, which exhibited a better distribution of fine and coarse aggregates. The bonded area started 50 mm away from the edge of the concrete block to avoid edge effects and exhibit a better distribution of fine and coarse aggregates [6]. Before installation, the concrete surface was grinded with an angle grinder to remove the thin smooth paste and expose the aggregate. The grinded surface was then cleaned from debris and dust (Figure 3(a)). The grinded surface was kept wet for one day prior to SRG application to ensure that the water-to-cement ratio in the matrix was not compromised by any hydration processes in the substrate. After the application of the first layer of grout (Figure 3(b)), the steel fabric was placed on top

of the layer and gently pressed by hand until it was fully impregnated in the mortar (Figure 3(c)). An additional layer of grout was then laid on top. This process was repeated more times for multi-ply SRG composites and, in these cases, special attention was paid to ensure that the strips were aligned with each other and that the time of application was within the working time of the mortar. Each grout layer had a thickness of 3 mm, which was controlled by specially designed moulds. Finally, the specimens were covered with a hessian fabric, which was kept wet for three days to enhance the hydration process. The specimens were left in laboratory conditions for at least 28 days before testing.

In this case, specimens were labelled using the notation "SB-X-Y-Z-N", in which "SB" denotes shear bond test, "X" denotes the concrete compressive strength ("L" for low and "M" for medium), "Y" denotes the density of steel fabric ("4" for S4 and "8" for S8), "Z" is the number of plies (1, 2 or 3), and finally, "N" identifies the specimen number (from 1 to 3 or 4) within a set of nominally identical specimens.

To apply the load, the free end of the steel fabric was sandwiched between aluminium plates measuring 120 mm × 100 mm using a two-part epoxy adhesive. In the case of multiple layers of steel fabrics, an additional 3 mm thick aluminium plate was placed between successive layers to keep their spacing similar to that within the bonded area. The aluminium plates were provided with holes to guarantee a uniform distribution of epoxy adhesive through the whole end-plate assembly area to prevent possible textile-to-plate sliding in the gripping area.

For the shear bond tests, a direct single pull-out shear setup was used. Specimens were placed in a reaction steel frame provided with an adjustable bed resting on four bolts (Figure 2(b)). The height and the level of the bed were controlled to ensure the alignment between the SRG strip and the gripping sandwich and prevent the development of stresses perpendicular to the load direction inside the composite and at the mortar-substrate interface. Moreover, the plate against which the concrete block was reacting, was fitted with a hemispherical joint to limit the possible misalignment resulting from imperfections in the moulds and errors during SRG installation. Finally, a T-cross section bracket attached to the reaction frame by means of two

bolts (Figure 2(b)) was used to restrain the back of the block from uplifting. Subsequently, a pre-loading load of 2 kN was applied to eliminate any slack in the unbonded textile.

The tests were carried out in displacement control at the rate of 0.01 mm/s [6] using a 50 kN load cell. To measure the slip between composite and substrate, two linear variable displacement transducers (LVDTs) were attached to the edges of the loaded end of the bonded area, while another two LVDTs were attached to the concrete block (see Figures 2(b) and 4). The LVDTs were reacting against a U-shaped bracket attached to the bare fabric at an offset of 10 mm from the loaded end. To estimate the slip rate, the relative composite-to-substrate displacement at the loaded end of the bonded area was then calculated as the difference between the average displacement of the LVDTs on the concrete block and that of those on the SRG. Digital image correlation (DIC) was also used to measure the slip and the strain in the unbonded textile by tracking the movement of small targets (3 mm diameter) attached at different locations near the loaded end of the bonded area. Figure 4 provides a schematic representation of the loaded end of the SRG composite with all DIC targets.

3 Results of direct tensile tests and lap-splice tests

3.1 Direct tensile tests

Tables 1 and 2 collect the results of the direct tensile and lap-splice tests for specimens with S4 and S8 textile, respectively. In these tables, the peak stress (f_t), the peak strain (ε_t), and the tensile modulus of elasticity in the uncracked stage (E_I) and in the cracked stage (E_{II}) are listed. The stress-strain response curves in Figure 5 display an initial linear stage, in which the mortar matrix was uncracked, followed by a second stage where multiple transversal through cracks developed. Once the crack pattern was stabilized (no new cracks appeared), the increase of external load was associated with an enlargement of existing cracks, until failure. Such a three-stage behaviour has already been observed on similar SRG composites comprising high-

strength cement or geopolymer mortars [1]. SRG composites with S4 textile failed by nearly simultaneous rupture of all cords. In the case of S8, however rupture of the cords occurred in a more progressive manner due to the more pronounced uneven load distribution across the larger number of cords.

3.2 Lap-splice tests

Lap-splice tests were characterized by an initial phase, in which the specimen was uncracked. Then the first (main) transversal crack developed at the end of the overlap on the side of the single textile layer. After this point, the width of the main crack increased with the increase of the applied load while other cracks progressively appeared on the portion of the coupon comprising one ply of textile (Figure 6(a)). On the contrary, the surface of the other portion remained uncracked. A longitudinal crack also appeared, and progressively extended, through the thickness of the coupon along the overlap (Figure 6(b)). All specimens failed by relative sliding between the textile layers, with the exception of only one specimen with S4 textile and 300 mm overlap length, in which rupture of the cords occurred.

Figure 7 illustrates the stress-slip response curves of the lap-splice tests. For better comparison, the peak stress values attained in the direct tensile tests and lap-splice tests on SRG specimens and their corresponding slip are plotted in Figure 8. The stress (f) in these figures is referred to one ply of textile, while the slip (s) is the relative displacement between the two portions of coupon separated by the main crack. As explained before, the main crack developed at the end of the overlap length, on the side of the coupon comprising one textile layer. To calculate such slip, two points on either side of the main crack were selected at the end of the test, and their relative displacement was derived from the DIC displacement field measurements. The values of peak stress (f_t) attained in lap-splice tests and direct tensile tests are also listed in Table 1 together with the ultimate slip (s_u), which is defined as the slip corresponding to f_t.

In the specimens comprising S4 textile, a brittle failure was observed with the shortest overlap length (L'=100 mm), whereas for L'=200 mm and L'=300 mm a nearly constant stress was detected after the peak, under increasing slip. In this phase of the test, the portion of the overlap involved in the load transfer process progressively shifted away from the main crack. The maximum stress reached by using L'=200 mm and L'=300 mm was similar to the SRG tensile strength, suggesting that the effective transfer length is between 100 mm and 200 mm. It should be considered that the peak stress in lap-splice tests might be expected to be slightly lower than that of direct tensile tests (in this study, by 9% on average) due to unavoidable misalignments and also the different clamping conditions of the textile on one side (at the overlap), which could cause an uneven stress distribution amongst the cords.

The response of SRG specimens with S8 textile was different from that of S4. The peak stress was lower (on average 37-39% of the tensile strength) due to the higher cord density, which let a smaller amount of mortar matrix pass through the cords and, therefore, led to a lower textile-to-textile load transfer capacity. As for S4, the effective transfer length for S8 was estimated to be between 100 mm and 200 mm.

4 Results of shear bond tests

4.1 Failure modes

The classification adopted by TC RILEM 250 CSM [23] was used to characterise the modes of failure of the bond test specimens (Fig. 9). Based on the experimental results, the following three distinct modes of failure were observed:

- Textile rupture (denoted as "E1"in Fig. 9) was characterised by the tensile failure of the steel cords immediately outside the bonded area (Figs. 10(a, b)), generally starting from an edge cord and propagating to the rest of the cords. This mode of failure was observed in the specimens with one layer of 4 cords/in textiles (SB-L-4-1, SB-M-4-1, Tables 3 and 4);

- Debonding at the matrix-to-substrate interface (denoted as “B” in Fig. 9) was observed mainly in the specimens with 2 and 3 layers of 4 cords/in textiles (SB-L-4-2, SB-L-4-3, SB-M-4-2, SB-M-4-3, Tables 3 and 4) and also in specimens with 3 layers of 8 cords/in textiles (SB-L-8-3, SB-M-8-3, Tables 3 and 4). The SRG strip was fully detached, while remaining almost intact with chunks of concrete substrate (Figs. 10(c, d)). This mode of failure occurred mainly when multiple layers were used and, although the better stress distribution within the composite helped in preventing a delamination type of failure, the average bond stress transferred to the concrete at the higher load levels reached the interface bond strength.;
- Debonding at the interface between the bottom layer of grout and the steel fabric (Figs. 10(e, f)) (denoted as “C” in Fig. 9) was observed in specimens with 1 and 2 layers of 8 cords/in textiles (SB-L-8-1, SB-L-8-2, SB-M-8-1, SB-M-8-2, Tables 3 and 4).

4.2 Stress-slip response

Tables 3 and 4 present the key results obtained from the shear bond tests, namely:

- The maximum load (P_{max}) and the associated maximum axial stress (f_{max}) in the textile. f_{max} is defined as:

$$f_{max} = \frac{P_{max}}{n * A_{cord}} \quad (1)$$

where n is the number of steel cords and A_{cord} is the cross sectional area of one cord.

- The slip at the loaded end of the SRG strip ($s_{com\ (LVDT)}$) obtained from the average value of relative displacement measured by the LVDTs (see Fig. 4) as follows:

$$s_{com(LVDT)} = \frac{\left(LVDT_{sub,l} - LVDT_{com,l}\right) + \left(LVDT_{sub,r} - LVDT_{com,r}\right)}{2} \quad (2)$$

- The slip at the loaded end of the SRG strip derived through DIC ($s_{com\ (DIC)}$), calculated as follows:

$$s_{com(DIC)} = \frac{\left(d_{com,l} - d_{sub,l}\right) + \left(d_{com,r} - d_{sub,r}\right)}{2} \quad (3)$$

where the distances $d_{sub,l}$, $d_{sub,r}$, $d_{com,l}$ and $d_{com,r}$ are defined in Fig. 4.

- The slip between the cords and the grout, s_{cor}, measured as the relative displacement between a DIC target attached to one cord and a target attached to the loaded end of the SRG bonded area, minus the elongation of the cord between these two targets (Eq. 4).

$$s_{cor} = \frac{(d_{cor,l1} - d_{com,l}) - (\varepsilon_{cor,l} \times L_{l2}) + (d_{cor,r1} - d_{com,r}) - (\varepsilon_{cor,r} \times L_{r2})}{2} \quad (4)$$

where

$$\varepsilon_{cor,l} = \frac{(d_{cor,l1} - d_{cor,l2})}{L_{l1}} \; and \; \varepsilon_{cor,r} = \frac{(d_{cor,r1} - d_{cor,r2})}{L_{r1}} \quad (5)$$

The definition of the various distances measured are depicted in Fig. 4. The slip values presented in Tables 3 and 4 correspond to the maximum load, P_{max}.

Figures 11-12 show the stress-slip response curves obtained from the LVDTs, whilst Figure 13 shows the average maximum load and the average maximum axial stress for the specimens with different number of layers, as well as the observed failure mode. The average slip at maximum load for specimens with different layers of SRG is presented in Figure 14.

The average stress-slip response curves obtained from DIC and LVDTs are compared in Figure 15(a). A good agreement between the two measurement methods was observed for the tests on SRG reinforcements comprising 1 and 2 textile plies, whereas in the case of 3 layers, the curves obtained from DIC showed a stiffer behaviour than those obtained from LVDTs. This stiffer behaviour was associated with slippage between the cords and the bracket that the LVDTs were reacting against, which resulted in exaggerated readings of the LVDTs compared to DIC system.

Data from DIC shows a small slip of steel cords inside the SRG (less than 0.23 mm) for all tested series, with the highest slip being associated with composites comprising one layer of the low-density steel textile (series SB-L-4-1 and SB-M-4-1) as shown in Figure 15 (b).

4.3 Influence of number of layers

The variation in the modes of failure observed in the SRG systems between 1 and 2, 3 layers of S4 textile (i.e. mode "E1" for one layer and mode "B" for 2 and 3 layers, see section 4.1) was not associated with clear changes in the average maximum load, which for the six specimen sets ranged between 17.5 kN and 20.5 kN (Tables 3 and 4). As a result of the addition of more plies, the peak axial stress reduced from 2170~2470N/mm^2 for 1 ply to 750~1150N/mm^2 for 2 and 3 plies (55~70% decrease). It should be noted that the test results were more scattered for multi-ply SRGs than for one ply. Based on the results obtained in this study, applying more than one layer of steel fabric with 4 cords/in does not increase the effective load capacity of the system.

In the case of SRG systems comprising S8 textile, the peak load (P_{max}) increased from 15 kN for 1 layer to 25~26 kN for 2 layers (62~73% increase) (Tables 3 and 4, series SB-L-8-1, SB-L-8-2, SB-M-8-1 and SB-M-8-2), while the same mode of failure was observed (mode "C" see section 4.1). The addition of a third layer changed the mode of failure to detachment at matrix-to-substrate interface (mode "B" see section 4.1) with the bond capacity reaching values of 26 and 29.5 kN for series SB-L-8-3 (Table 3) and SB-M-8-3 (Table 4), respectively. The change in the mode of failure from "C" to "B" is mainly attributed to the lower stress per cord and the lower bond stress between the cord and the mortar. However, the bond stress at the mortar – concrete interface reached higher stresses and failed. As for the peak axial stress in the textile, passing from 1 to 2 plies was associated to a reduction from 940~960N/mm^2 to 780~813N/mm^2 (13~19% reduction), respectively, whereas the addition of the third layer entailed a further decrease by 25~31% (the peak axial stress was 540~610N/mm^2 and the reduction with respect to 1 ply was 35~44%).

Finally, increasing the number of textile layers reduced the ultimate slip in the specimens strengthened with the low-density steel fabric. More specifically, in series SB-M-4, $s_{com\ (LVDT)}$ reduced, on average, from 1.9 mm (1 ply) to 1.0 mm (2 plies) and to 0.6 mm (3 plies) (Table 4),

whereas for SB-L-4, $s_{com\ (LVDT)}$ reduced, on average from 1.9 mm (1 ply) to 0.8 mm (2 plies) and to 0.9 mm (3 plies) (Table 3). On the contrary, the effects on the ultimate slip detected for SRG systems with S8 textile were less significant due to the changes in the mode of failure ($s_{com\ (LVDT)}$ being 0.82~1 mm for SB-M-8 (Table 4) and 0.65~0.74 mm for SB-L-8 (Table 3)).

4.4 Influence of textile density

The influence of textile density on the SRG-to-substrate load transfer mechanism has already been investigated in several studies that dealt with one-ply systems [e.g. 12]. In general, the larger spaces between the cords of the lower density textiles (S4) allow a larger amount of mortar to pass through the textile, which results in a better interlaminar shear capacity with respect to denser fabrics [1]. Analogous considerations can be made for any FRCM, independently from the utilised textile material [16]. The results achieved in the present investigation are consistent with existing literature.

SRG composites with one ply of S4 textile exhibited an average maximum load of approximately 19 kN (series SB-L-4-1 and SB-M-4-1, Tables 3 and 4), which was slightly higher than that of the systems with one ply of S8 (15 kN, series SB-L-8-1 and SB-M-8-1, Tables 3 and 4). The larger cross sectional area of S8 textile with respect to S4 highlights the influence of textile density on SRG effectiveness, since the peak axial stress of SRGs with S4 was, on average, 2.5 times higher than that with S8 (Table 4). In terms of failure mode, all specimens with one ply of S4 textile exhibited cord rupture (mode "E1") except from specimen SB-M-4-1-2, which failed by composite-to-substrate debonding (mode "B") at a lower failure load (12kN). The specimens with S8 textile (SB-L-8-1 and SB-M-8-1 series), instead, failed by debonding at the interface between fabric and matrix (mode "C").

Textile density affected the trends associated with the increase of plies (see Figures 13 and 14 and see also comments in Section 4.3). SRG systems with S4 textile exhibited similar peak loads independently from the number of plies, which was associated with a nearly linear reduction of peak axial stress with the increase in the number of textile plies. Furthermore, the

failure mode changed from tensile rupture (mode "E1" Fig. 9) for 1-ply systems to debonding at the interface with the substrate (mode "B" Fig. 9) for multi-ply systems. On the contrary, composites with S8 exhibited an increase of peak load and a less pronounced decrease of stress, with a quasi-stabilization for multi-ply systems, as the increase of P_{max} was proportional to the increase of cross-sectional area when passing from 2 to 3 plies. It is worth noting that the peak axial stress attained by SRGs with S4 was always higher than that with S8. Finally, for these specimens failure occurred at the interface between fabric and matrix (mode "C") for 1 and 2 plies, and between matrix and substrate (mode "B") for 3-ply SRGs.

The density of the steel textile affected the ultimate slip of the specimens strengthened with only one layer of textile. There was a reduction of approximately 60% and 50% in the ultimate slip when increasing the density of steel textile from 4 to 8 cords/in for series SB-L and SB-M, respectively. On the other hand, specimens strengthened with 2 and 3 layers exhibited a slight change in terms of ultimate slip when the textile density was increased from 4 to 8 cords/in.

4.5 Influence of concrete compressive strength

As seen in Tables 3 and 4, half of the tested specimens failed due to detachment at the substrate-to-matrix interface ("B"), suggesting that the mechanical properties of the concrete substrate may play a role in the bond behaviour of the composite system. However, from the tests results obtained in this study, no solid conclusions can be drawn on the influence of concrete compressive strength due to the complex nature of shear bond test, particularly when multiple layers of steel textile reinforcement are applied. Possible imperfections in fabrication might have introduced misalignments between the different textiles layers, thus resulting in a non-uniform distribution of stresses, and thus to variation of the modes of failures between detachment at matrix-to-substrate (mode "B") and textile-to-matrix interface (mode "C" Fig. 9). Considering the modes of failures observed and the overall behaviour of the specimens, the high difference in compressive strength between the mortar and the substrate concrete (especially the 14 kN/m^2 case) did not have a negative impact on the composite behaviour of the interface.

5. Conclusions

An experimental study was performed on the bond behaviour of SRG systems comprising multiple layers of galvanized UHTSS textiles and a geopolymer mortar. Two different textiles were used with 4 cords/in and 8 cords/in density. First lap-splice tests were conducted to provide information on the textile-to-textile load transfer capacity. The effective transfer length was found to be between 100 mm and 200 mm for both fabrics. Further increase of the overlap length did not improve the load transfer capacity but led to a larger ultimate relative slip associated with a progressive shifting of the overlap area effectively involved in the load transfer process. Textile density highly affected the textile-to-textile bond capacity, which was higher for the SRG composites with 4 cords/in than for those with 8 cords/in, demonstrating that the textile-to-textile bond capacity relies on the amount of mortar passing through the voids between the cords.

Subsequently, single-lap shear bond tests provided information on the bond performance on concrete substrates. SRG systems comprising 4 cords/in textiles exhibited similar peak load values independently from the number of plies, and accordingly, the stress at detachment decreased linearly with the increase of the number of layers. The use of multi-ply SRG with low density textile, therefore, does not appear to be very effective for flexural strengthening applications. As for the failure mode, cord rupture (1 ply) was changed to debonding at the SRG-to-substrate interface (2 and 3 plies). The use of multiple layers of steel textile with 8 cords/in led to an increase of the maximum load that can be transferred from the SRG system to the substrate. Specimens with 1 and 2 plies failed by textile-to-matrix detachment, whereas in those with 3 plies failure took place at the interface between concrete substrate and SRG strip. The gain in strength with the increase of the number of layers was less than linear, which was associated with a decrease of the peak axial stress, indicating a lower efficiency of multi-ply SRGs with respect to those with one fabric layer. The concrete substrate was involved in the mode of failure (matrix-to-substrate interface) for 50% of the tested

specimens. However, it was not clear what is the influence of the concrete compressive strength on the bond behaviour due to the complex nature of shear bond tests with multiple layers.

Further investigation is still needed on the bond behaviour of multi-ply SRG reinforcements in order to estimate their effectiveness, assess the ultimate strength of retrofitted structural members, and develop design formula that are oriented to the optimized use of reinforcement materials. With the aim of fostering the use of SRG in engineering practice, careful installation procedures should be followed (e.g., by wetting and cleaning the application surface) and wet curing conditions should be ensured. Furthermore, the possibility of enhancing the bond behaviour by specific substrate preparation (grinding, consolidation, primer application) and/or strengthening details (such as the use of mechanical connectors) deserves supplementary research efforts for a further improvement of the proposed strengthening technology.

Acknowledgments

The materials for this investigation (steel textiles and mortar) were provided by Kerakoll S.p.A. (Sassuolo, MO, Italy). S.A. would like to thank Shaqra University in Saudi Arabia and Saudi Arabian Cultural Bureau in the UK for funding this part of his PhD research. S.D.S., G.d.F. and F.R. acknowledge funding from Regione Lazio for the Research Project “SICURA Sustainable technologies for the seismic protection of the cultural heritage” (2018-2020) and from the Italian Ministry of Education, University and Research (MIUR), for the grant attributed to the Department of Engineering of Roma Tre University, in the frame of the Departments of Excellence Initiative (2018-2022).

References

1. S. De Santis, F. Ceroni, G. de Felice, M. Fagone, B. Ghiassi, A. Kwiecień, G. Lignola, M. Morganti, M. Santandrea, M. Valluzzi, A. Viskovic. Round Robin Test on tensile and bond behaviour of Steel Reinforced Grout systems. Compos B Eng 2017b: 127: 100-120.

2. G.E. Thermou, S.J. Pantazopoulou, A.S. Elnashai. Global interventions for seismic upgrading of substandard RC buildings. J Struct Eng 2012; 138(3): 387-401.

3. M. Matana, A. Nanni, L.R. Dharani, P. Silva, G. Tunis. Bond Performance of steel reinforced polymer and steel reinforced grout. In: Proceedings of BBFS Conference. Hong Kong, December, 2005.

4. X. Huang, V. Birman, A. Nanni, G. Tunis. Properties and potential for application of steel reinforced polymer and steel reinforced grout composites. Compos B Eng 2005; 36 (1): 73-82.

5. G. de Felice, S. De Santis, L. Garmendia, B. Ghiassi, P. Larrinaga, P.B. Lourenço, D.V. Oliveira, F. Paolacci, C.G., Papanicolaou. Mortar-based systems for externally bonded strengthening of masonry. Mater Struct 2014; 47(12): 2021-2037.

6. L. Ascione, G. de Felice, S. De Santis. A qualification method for externally bonded Fibre Reinforced Cementitious Matrix (FRCM) strengthening systems. Compos B Eng 2015; 78: 497-506

7. J. Donnini, V. Corinaldesi, A. Nanni. Mechanical properties of FRCM using carbon fabrics with different coating treatments. Compos B Eng 2016; 88: 220-228

8. E. Stievanin, F. Da Porto, M. Panizza, E. Garbin, C. Modena. Bond characterization between historical concrete substrate and SRG/SRP strengthening systems. In: Proceedings of SEMC Conference. Cape Town, September, 2013.

9. F. Bencardino, A. Condello, A. F. Ashour. Single-lap shear bond tests on Steel Reinforced Geopolymeric Matrix-concrete joints. Compos B Eng 2017; 110: 62-71

10. F. Ascione, M. Lamberti, A. Napoli, R. Realfonzo. Experimental bond behavior of Steel Reinforced Grout systems for strengthening concrete elements. Constr Build Mater 2020; 232: 117105

11. A. Razavizadeh, B. Ghiassi, D. V. Oliveira. Bond behaviour of SRG-strengthened masonry units: Testing and numerical modelling. Constr Build Mater 2014; 64: 387-397.

12. S. De Santis, G. de Felice. Steel reinforced grout systems for the strengthening of masonry structures. Compos Struct 2015; 134: 533-548.

13. S. De Santis. Bond behaviour of Steel Reinforced Grout for the extrados strengthening of masonry vaults. Constr Build Mater 2017; 150: 367-382

14. A. Bilotta, F. Ceroni, E. Nigro, M. Pecce. Experimental tests on FRCM strengthening systems for tuff masonry elements. Constr Build Mater 2017; 138: 114-133.

15. S. De Santis, F. Carozzi, G. de Felice, C. Poggi. Test methods for Textile Reinforced Mortar systems. Compos B Eng 2017a; 127: 121-132.

16. G. de Felice, G., D'Antino, A., De Santis, S., Meriggi, P., Roscini, F. Lessons learned on the tensile and bond behaviour of Fabric Reinforced Cementitious Matrix (FRCM) composites. Frontiers in Built Environment 2020; 6: 5.

17. G. de Felice G, Aiello MA, Caggegi C, Ceroni F, De Santis S, Garbin E, Gattesco N, Hojdys Ł, Krajewski P, Kwiecień A, Leone M, Lignola GP, Mazzotti C, Oliveira D, Papanicolaou C, Poggi C, Triantafillou T, Valluzzi MR, Viskovic A. Recommendation of RILEM TC 250-CSM: Test method for Textile Reinforced Mortar to substrate bond characterization. Mater Struct 2018; 51 (4): 95.

18. A. Napoli, R. Realfonzo. Reinforced concrete beams strengthened with SRP/SRG systems: Experimental investigation. Constr Build Mater 2015; 93: 654-677.

19. Products.kerakoll.com. 2020. Technical Data Sheet For Geo-Lite Mortar. [online] Available at: https://products.kerakoll.com/yep-repository/kerakoll/media/Geolite__rating_2019_EN.pdf [Accessed 24 April 2020].

20. S. De Santis S, Hadad HA, De Caso y Basalo FJ, de Felice G, Nanni A. Acceptance Criteria for Tensile Characterization of Fabric Reinforced Cementitious Matrix (FRCM) Systems for Concrete and Masonry Repair. J Compos Const 2018; 22(6): 04018048. DOI: 10.1061/(ASCE)CC.1943-5614.0000886.

21. M. Tekieli, S. De Santis, G. de Felice, A. Kwiecień, F. Roscini. Application of Digital Image Correlation to composite reinforcements testing. Compos Struct 2017; 160: 670-688.

22. fib bulletin 24 (2003). “Seismic assessment and retrofit of reinforced concrete buildings.” State of the art report, Task Group 7.1, fédération internationale du béton (fib).

23. G. de Felice, M.A. Aiello, C. Caggegi, et al. Recommendation of RILEM Technical Committee 250-CSM: Test method for Textile Reinforced Mortar to substrate bond characterization. Mater Struct 2018; 51: 95

Figures

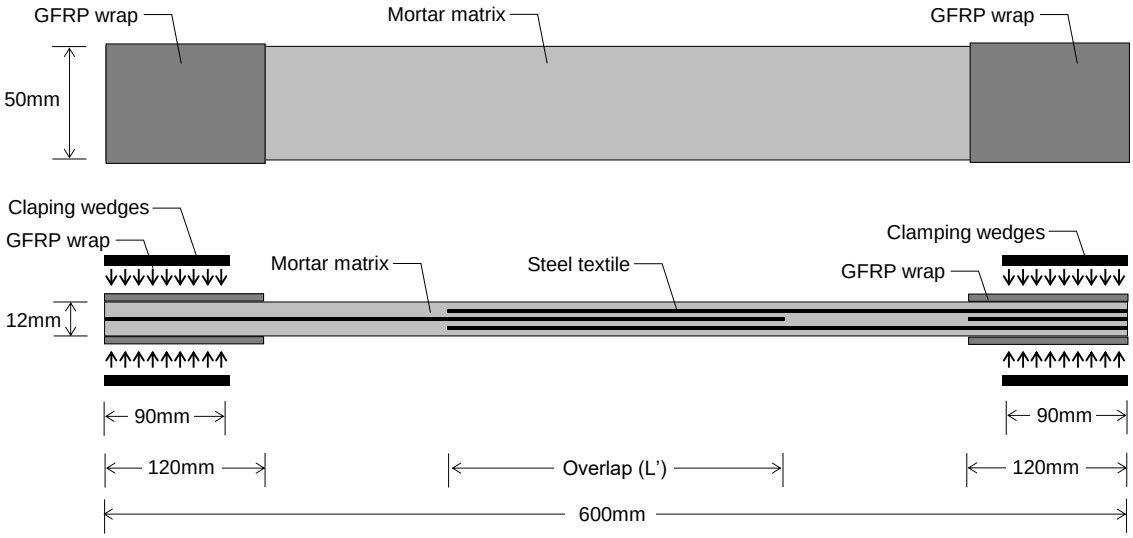

Figure 1. Top and side view of SRG specimens for lap-splice tests.

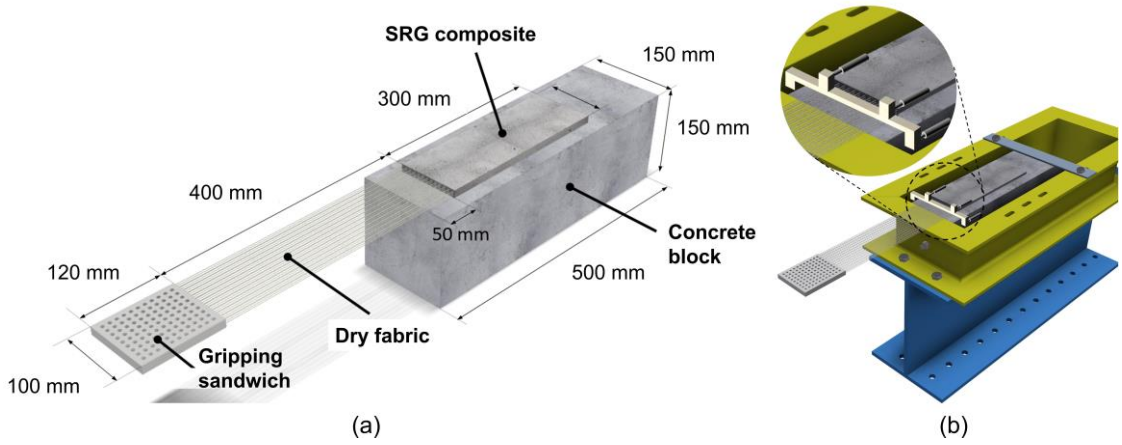

Figure 2. (a) Geometry of specimens and (b) setup of single-lap shear bond test with a zoomed view on the loaded area.

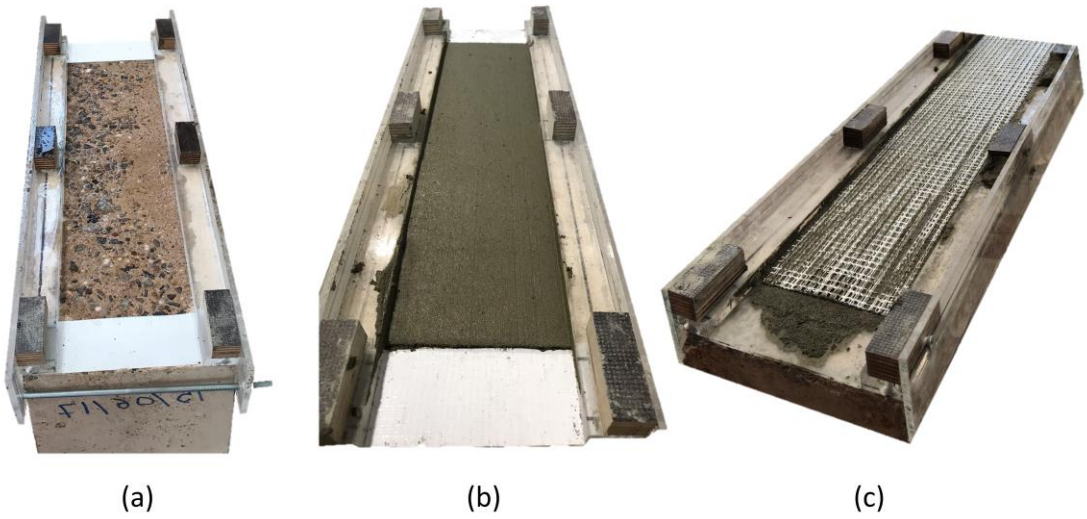

Figure 3. Steps of the manufacturing process of specimens for shear bond tests: (a) grinded surface prior to the application of the first layer of grout, (b) application of the first layer of grout, and (c) first layer of steel textile placed on top of the grout layer.

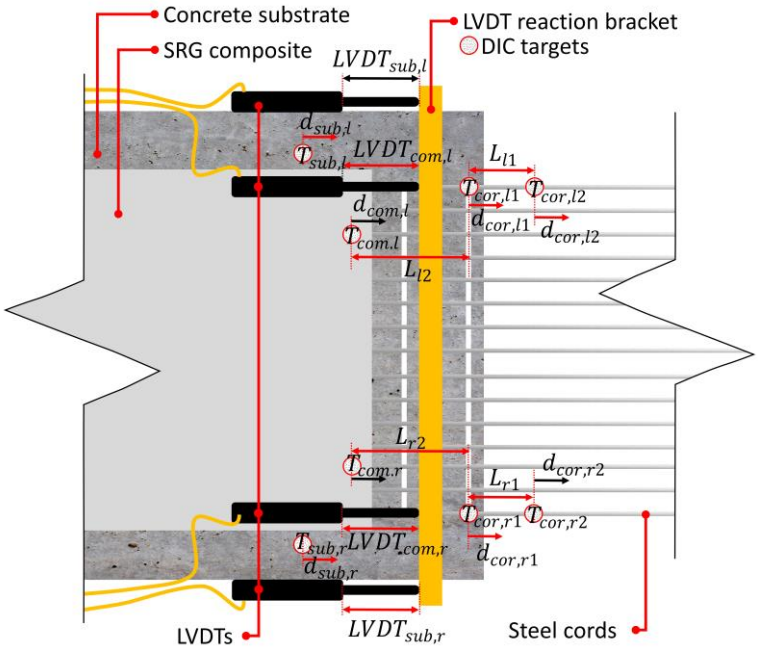

Figure 4. Schematic presentation of the properties (slip of composite, slip of cords, and strain in cords) measured by using DIC system.

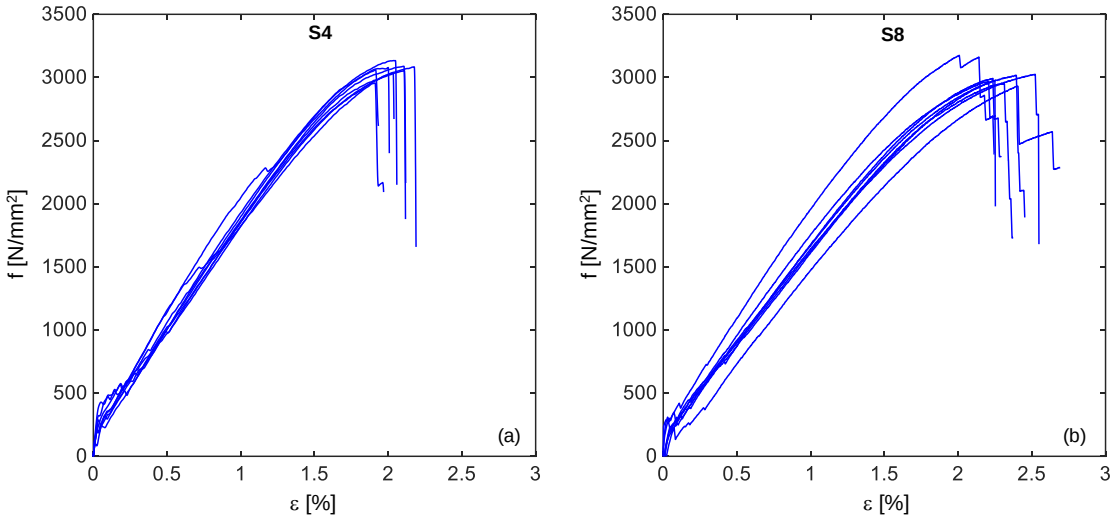

Figure 5. Stress-strain response curves of direct tensile tests on SRG coupons comprising (a) S4 and (b) S8 textiles.

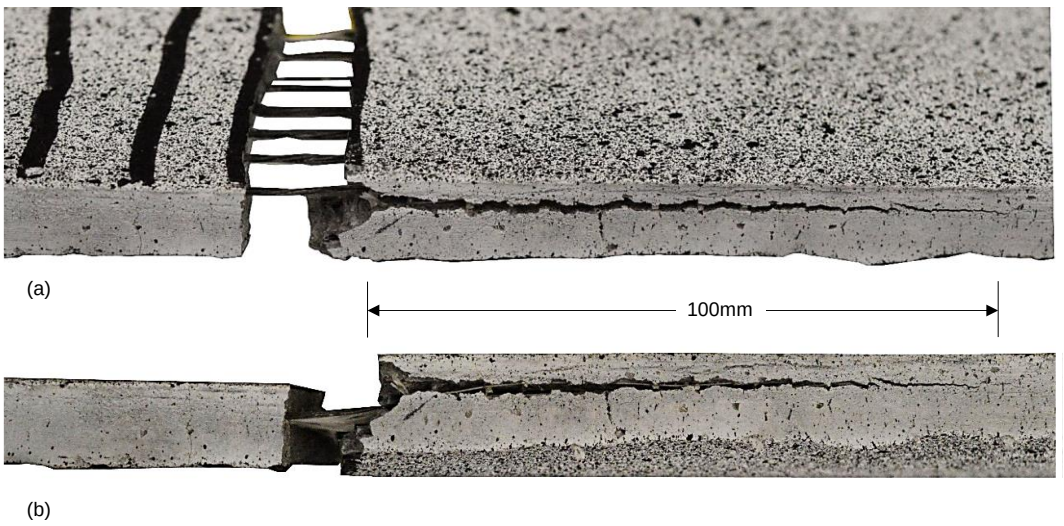

Figure 6. (a) Isometric and (b) side views of the crack pattern observed in lap-splice tests (LS-4-100-2 specimen).

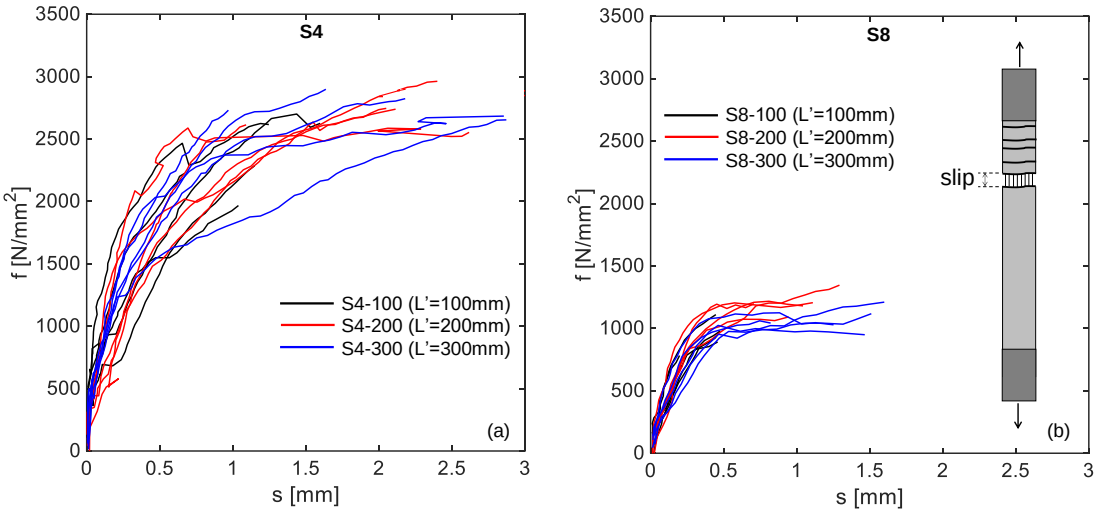

Figure 7. Stress-slip response curves of lap-splice tests on SRG specimens comprising (a) S4 and (b) S8 textiles.

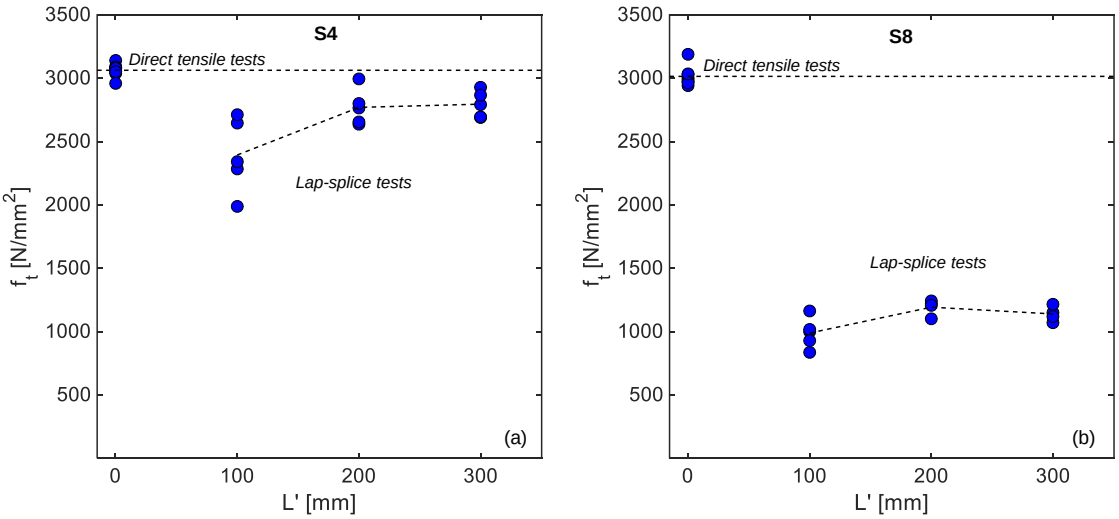

Figure 8. Peak stress attained in direct tensile tests and in lap-splice tests on SRG specimens comprising (a) S4 and (b) S8 textiles.

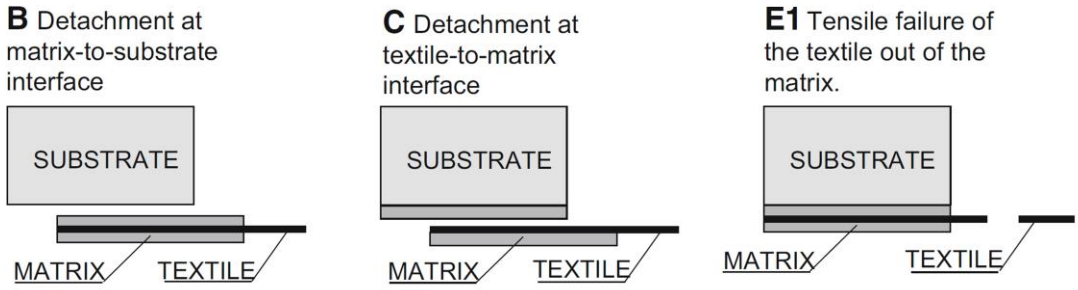

Figure 9. Modes of failure observed in the bond tests according to TC RILEM 250 CSM [23].

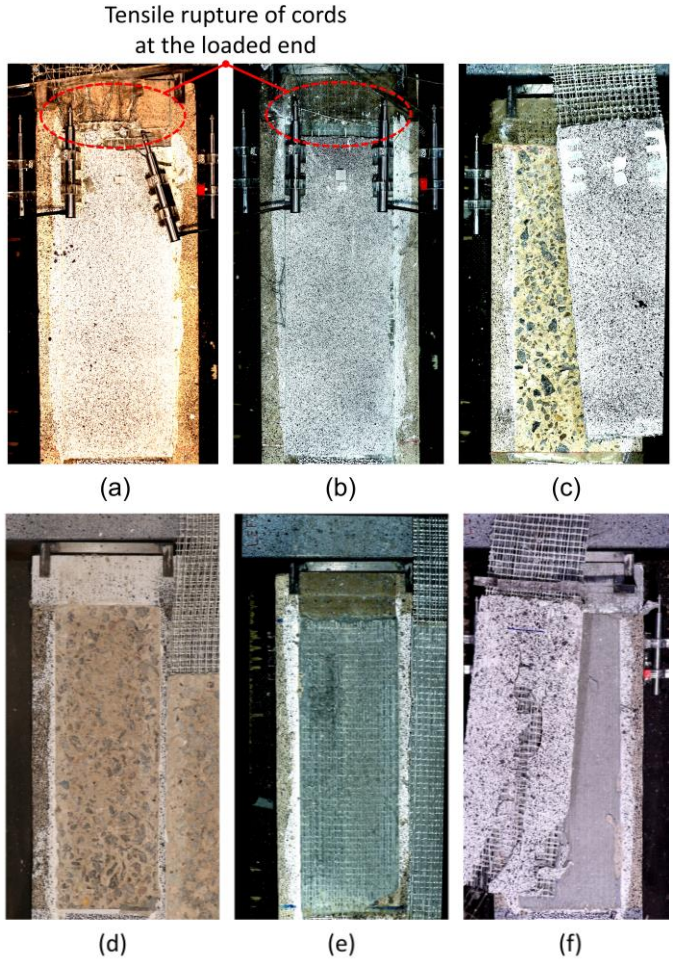

Figure 10. Failure modes detected in shear bond tests: fabric rupture [Mode E1] in (a) SB-L substrates and (b) SB-M substrates, debonding at the substrate-to-matrix interface [Mode B] in (c) SB-L substrates and (d) SB-M substrates, detachment and the textile-to-matrix interface [Mode C] in (e) SB-L substrates and (f) SB-M substrates.

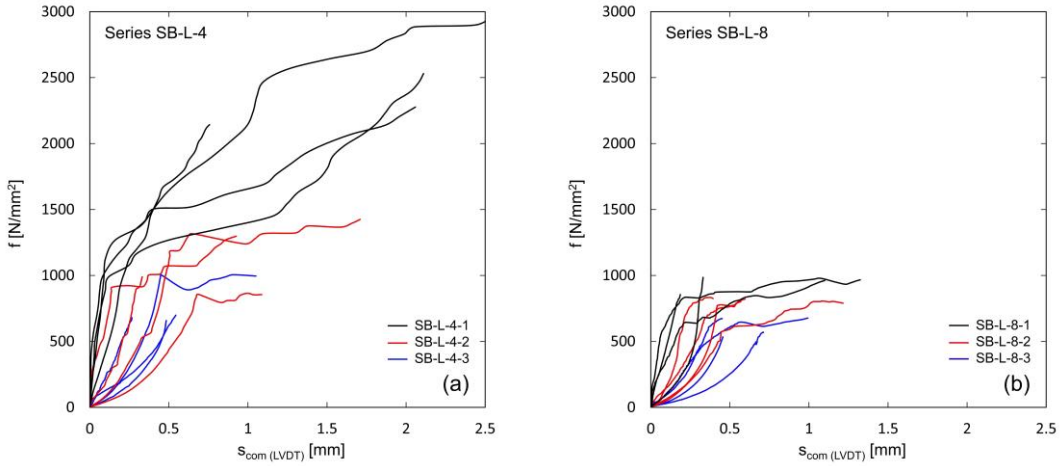

Figure 11. Stress-slip response curves of shear bond tests on low compressive strength substrate: (a) SB-L-4 and (b) SB-L-8 series.

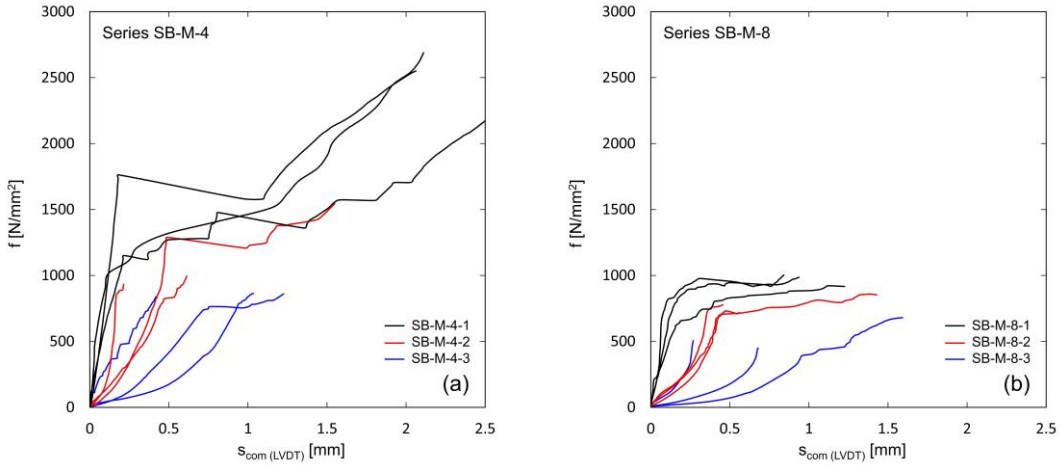

Figure 12. Stress-slip response curves of shear bond tests on medium compressive strength substrate: (a) SB-M-4 and (b) SB-M-8 series.

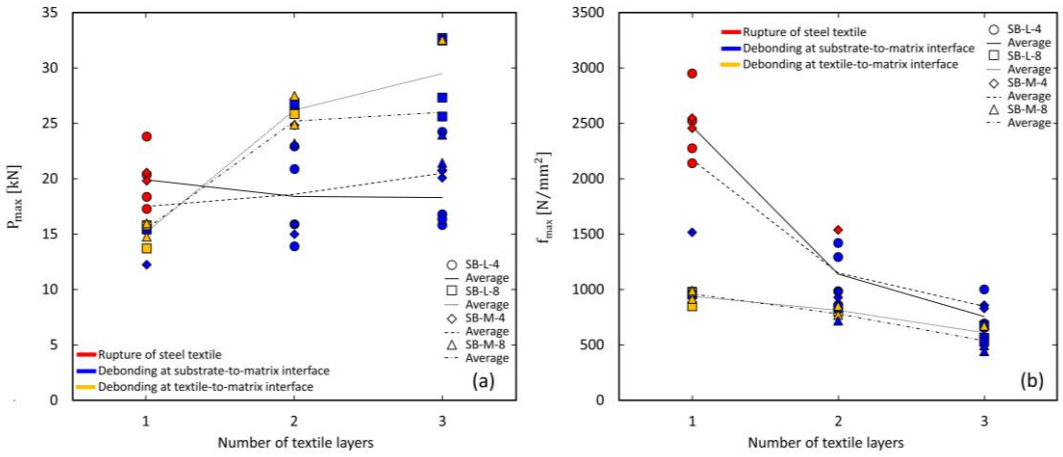

Figure 13. (a) Peak load and (b) peak axial stress attained in shear bond tests vs. number of textile layers.

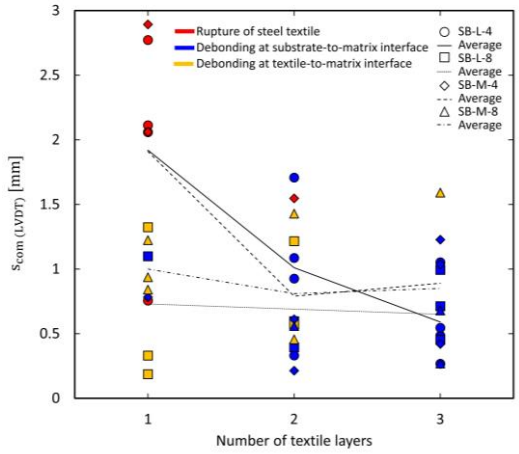

Figure 14. Corresponding slip attained in shear bond tests vs. number of textile layers.

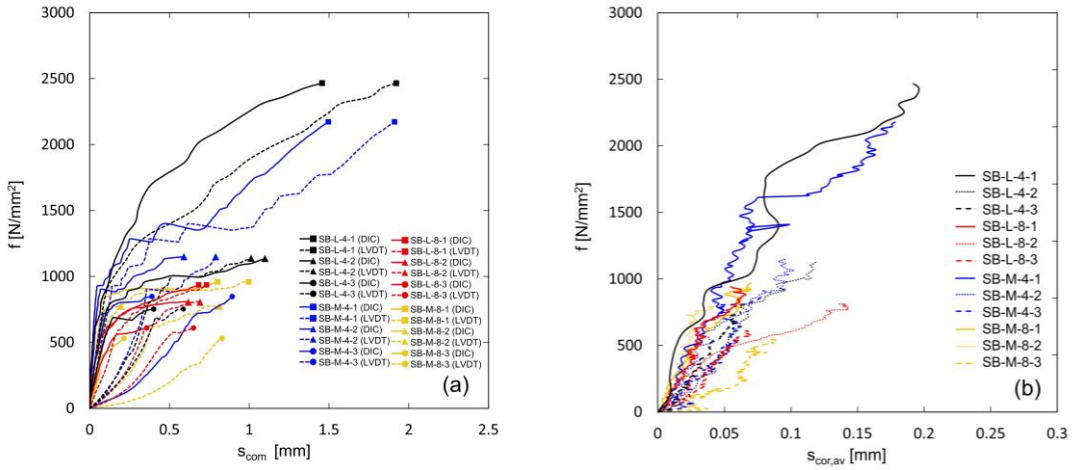

Figure 15. The average stress-slip of composite response curves obtained from DIC system and LVDTs and (b) the average stress-slip of cords response curves.

Tables

Table 1. Results of direct tensile tests and lap-splice tests for specimens with S4 textile.

Group	Specimen	f_t N/mm^2	ε_t %	E_I kN/mm^2	E_{II} kN/mm^2	s_u mm
DT-4	1	3134.6	2.05	1815	178.5	
	2	3089.4	2.12	1885	170.6	
	3	3084.2	2.19	1658	164.8	
	4	3041.5	2.06	1701	172.0	
	5	3054.5	2.13	1688	172.8	
	6	2958.6	1.93	1640	188.7	
	7	3080.3	2.04	1601	181.1	
	8	3063.8	1.95	1718	194.5	
	Average	3063.3	2.06	1713.3	177.9	
	St. dev.	50.7	0.09	93.9	9.9	
	CV (%)	2	4	5	5	
LS-4-100	1	2224.3				0.67
	2	2624.3				1.19
	3	1966.9				1.04
	4	2286.3				1.15
	5	2700.3				1.44
	Average	2360.4				1.10
	St. dev.	301.7				0.28
	CV (%)	13				25
LS-4-200	1	2739.3				2.11
	2	2588.1				0.69
	3	2745.7				2.05
	4	2962.7				2.40
	5	2613.6				1.09
	Average	2729.9				1.67
	St. dev.	148.4				0.74
	CV (%)	5				44
LS-4-300	1	2730.7				0.97
	2	2898.5				1.64
	3	2653.7				2.87
	4	2804.2				2.11
	5	2683.7				2.86
	Average	2754.2				2.09
	St. dev.	98.7				0.82
	CV (%)	4				39

Table 2. Results of direct tensile tests and lap-splice tests for specimens with S8 textile.

Group	Specimen	f_t N/mm^2	ε_t %	E_I kN/mm^2	E_{II} kN/mm^2	s_u mm
DT-8	1	2973.5	2.21	1651	181.4	
	2	3188.1	2.01	1655	190.6	
	3	3002.4	2.24	1901	172.7	
	4	2959.3	2.25	1855	169.7	
	5	3028.1	2.39	1499	174.0	
	6	2942.7	2.40	1888	169.6	
	7	2961.8	2.31	1653	169.5	
	8	3034.4	2.49	1403	156.1	
	Average	3011.3	2.29	1688.1	172.9	
	St. dev.	78.8	0.15	182.8	10.0	
	CV (%)	2	6	11	6	
LS-8-100	1	2224.3				0.47
	2	2624.3				0.45
	3	1966.9				0.48
	4	2286.3				0.46
	5	2700.3				0.20
	Average	2360.4				0.41
	St. dev.	301.7				0.12
	CV (%)	13				29
LS-8-200	1	1206.0				1.11
	2	1217.2				0.81
	3	1091.9				0.94
	4	1346.2				1.29
	5	1197.1				0.71
	Average	1211.7				0.97
	St. dev.	90.4				0.23
	CV (%)	7				24
LS-8-300	1	1060.6				0.75
	2	1124.8				0.88
	3	1210.2				1.60
	4	1117.4				1.51
	5	1023.7				0.46
	Average	1107.4				1.04
	St. dev.	71.0				0.49
	CV (%)	6				48

Table 3. Results of shear bond tests on low compressive strength concrete substrates (series SB-L).

Group	Specimen	P_{max} kN	f_{max} N/mm^2	$s_{com(LVDT)}$ mm	$s_{com\ (DIC)}$ mm	$s_{cor\ (DIC)}$ mm	MoF
SB-L-4-1	1	17.27	2140	0.76	0.69	0.24	E1
	2	20.35	2522	2.11	1.22	0.12	E1
	3	18.36	2275	2.06	0.94	0.31	E1
	4	23.81	2951	2.77	2.98	0.21	E1
	Average	19.95	2472	1.93	1.46	0.22	E1
	St. dev.	2.87	356	0.84	1.04	0.08	
	CV (%)	15	15	44	72	37	
SB-L-4-2	1	13.90	861	1.09	0.91	0.16	B
	2	22.92	1420	1.71	1.77	0.14	B
	3	15.89	984	0.33	0.29	0.12	B
	4	20.88	1294	0.93	1.43	0.08	B
	Average	18.40	1140	1.02	1.1	0.13	B
	St. dev.	4.21	261	0.57	0.65	0.03	
	CV (%)	23	23	56	60	24	
SB-L-4-3	1	24.24	1001	1.05	1.15	0.06	B
	2	15.82	653	0.48	0.14	0.15	B
	3	16.79	694	0.55	0.17	0.04	B
	4	16.35	675	0.27	0.15	0.04	B
	Average	18.3	756	0.59	0.4	0.07	B
	St. dev.	3.98	164	0.33	0.5	0.05	
	CV (%)	22	22	56	125	72	
SB-L-8-1	1	13.71	849	0.19	0.11	0.03	C
	2	15.81	979	0.33	0.2	0.05	C
	3	15.69	972	1.32	1.33	0.12	C
	4	15.42	955	1.1	1.12	0.11	B-C
	Average	15.16	939	0.74	0.69	0.08	C
	St. dev.	0.98	61	0.56	0.62	0.04	
	CV (%)	7	7	76	90	50	
SB-L-8-2	1	26.34	816	0.6	0.51	0.12	B
	2	25.87	801	1.22	0.93	0.3	C
	3	25.84	801	0.57	0.24	0.09	C
	4	26.84	832	0.39	0.8	0.09	B-C
	Average	26.22	813	0.7	0.62	0.15	C
	St. dev.	0.47	15	0.36	0.31	0.1	
	CV (%)	2	2	52	50	67	
SB-L-8-3	1	27.32	564	0.71	0.18	0.09	B
	2	25.62	529	0.46	0.2	0.03	B
	3	32.71	676	0.99	0.64	0.1	B
	4	32.48	671	0.45	0.42	0.08	B
	Average	29.53	610	0.65	0.36	0.08	B
	St. dev.	3.6	75	0.26	0.22	0.03	
	CV (%)	13	13	40	62	38	

Table 4. Results of shear bond tests on medium compressive strength concrete substrates (series SB-M).

Group	Specimen	P_{max} kN	f_{max} N/mm^2	$s_{com\ (LVDT)}$ mm	$s_{com\ (DIC)}$ mm	$s_{cor\ (DIC)}$ mm	MoF
SB-M-4-1	1	20.56	2548	2.06	1.66	0.19	E1
	2	12.24	1516	0.78	0.26	0.2	B
	3	19.82	2456	2.89	2.57	0.16	E1
	Average	17.54	2173	1.91	1.5	0.18	E1
	St. dev.	4.6	571	1.06	1.16	0.02	
	CV (%)	27	27	56	78	12	
SB-M-4-2	1	14.99	929	0.21	0.12	0.1	B
	2	24.83	1538	1.55	1.51	0.17	E1
	3	15.87	983	0.61	0.14	0.06	B
	Average	18.56	1150	0.79	0.59	0.11	B
	St. dev.	5.44	337	0.69	0.8	0.06	
	CV (%)	30	30	88	136	55	
SB-M-4-3	1	20.72	856	1.23	0.43	0.1	B
	2	20.78	858	1.04	0.07	0.06	B
	3	20.08	829	0.42	0.68	0.14	B
	Average	20.53	848	0.9	0.39	0.1	B
	St. dev.	0.39	16	0.42	0.31	0.04	
	CV (%)	2	2	47	80	40	
SB-M-8-1	1	14.76	915	1.22	N/A	N/A	C
	2	15.79	978	0.94	0.86	0.04	C
	3	15.98	990	0.84	0.75	0.13	C
	Average	15.51	961	1	0.81	0.09	C
	St. dev.	0.66	40	0.2	0.08	0.06	
	CV (%)	5	5	20	10	67	
SB-M-8-2	1	27.48	851	1.43	N/A	N/A	C
	2	24.90	771	0.46	0.2	0.05	C
	3	23.19	719	0.56	N/A	N/A	B
	Average	25.19	780	0.82	0.2	0.05	C
	St. dev.	2.16	66	0.53			
	CV (%)	9	9	65			
SB-M-8-3	1	32.54	672	1.59	0.54	0.16	C
	2	21.43	443	0.68	0.07	0.04	B
	3	23.97	495	0.27	0.08	0.11	B
	Average	25.98	537	0.85	0.23	0.1	B
	St. dev.	5.82	120	0.68	0.27	0.06	
	CV (%)	23	23	80	118	60	